Nuclear Inst. and Methods in Physics Research, A 984 (2020) 164571

Contents lists available at ScienceDirect

Nuclear Inst. and Methods in Physics Research, A

journal homepage: www.elsevier.com/locate/nima

Analysis of sampling and noise error on the energy measurement of direct digitally acquired pulsed signals

Irene Degl'Innocenti [a,b,*], Andrea Boccardi [a], Luca Fanucci [b], Manfred Wendt [a]

[a] CERN, European Organization for Nuclear Research, CH-1211 Geneva 23, Switzerland
[b] Department of Information Engineering, Università di Pisa, Via Girolamo Caruso, 16, 56122 Pisa PI, Italy

ARTICLE INFO

Keywords:
Beam position monitor
Estimation error
Sampling distortion
Power measurement
Direct digitization
Gaussian noise

ABSTRACT

The precise measurement of the energy content of a pulse signal, limited in time and bandwidth, is of great interest in many applications, and can be achieved by direct digitization of the analog signal, followed by calculation of the mean squared amplitude of the data samples. The beam position measurement in a particle accelerator is among the applications, and this technique is proposed for the next generation of read-out electronics for the beam position monitors of the CERN Large Hadron Collider. The analog-to-digital converter is a key component of the signal processing chain, and defines the performance of the measurement through its characteristics and features, in particular the maximum sampling rate and the effective number of bits. This paper analyzes the error on the measurement of the signal energy for a specific pulse waveform within a given time window, caused by the analog-to-digital converter sampling effects due to the finite, unsynchronized sampling rate. In a following step the result is combined with the effect of a noisy analog-to-digital converter of finite resolution. This gives a general expression for the signal-to-noise ratio, which can be used to find the optimal trade-off between sampling rate and resolution of an analog-to-digital converter for any given single pulse waveform.

1. Introduction

The precise, reproducible measurement of the energy of an analog, single pulse waveform is of general interest in many technical applications. In the field of particle accelerator beam instrumentation it is widely used to measure single bunch parameters such as intensity, position and profile. One application is for the measurement of the beam position, which is based on electromagnetic beam pickups, so-called beam position monitors (BPM), which are distributed throughout the accelerator, in strategic points of the machine layout. Each BPM transforms the electromagnetically coupled signal from the beam into a set of four analog signals that can be combined to give information about the horizontal and vertical beam position. The initial electromagnetically coupled signals are typically on the same timescale as the length of the traversing charged, particle bunch which, for the Large Hadron Collider (LHC), is in the order of 1 ns. A change in the beam position or in the beam intensity will result in a change of the amplitude (or energy) of these pickup signals, while the shape of the waveform remains the same [1].

The advances in the technology of analog-to-digital converters (ADC) now enable the energy measurement of short, pulsed, electrical signals through their direct digitization. In this context, the specifications and performance of the ADC play a critical role, and to a large extent define the overall quality of the measurement. The choice of the ADC is therefore a key element of the instrument design. The trade-off between achievable resolution and maximum sampling rate has a fundamental impact on the quality of the energy measurement of short, pulsed signals, and is discussed in detail in the following sections.

The analysis of the effect of sampling on waveform distortion is a classic problem extensively discussed in signal processing and information theory. In [2] *Shannon* introduced a sampling rate theory in the presence of noise, providing an expression for the minimum sampling rate required to remain within a given target distortion for a bandlimited *Gaussian* source. In [3] he demonstrated that a minimum sampling frequency exists, beyond which any continuous, band-limited, noiseless signal can be reconstructed without error from its samples. Such minimum frequency is named *Nyquist* rate (R_{Nyq}) and for a signal with bandwidth B (the signal spectrum respects the condition $|X(f)| = 0$ for $f > B$) it is equal to twice the bandwidth ($R_{Nyq} = 2B$).

For short, pulsed signals, the sampling frequency required by the *Nyquist–Shannon* theorem for error free reconstruction is often not achievable, being limited by the available ADC technology. *Matthews* [4] and *Kipnis, et al.* [5] analyzed the effect of uniform sampling distortion on a noisy, stationary *Gaussian* random process, in the case of sub-*Nyquist* sampling, using a variety of proofing techniques. *Mohammadi* and *Marvasti* [6] studied the trade-off between sampling frequency

* Corresponding author at: CERN, European Organization for Nuclear Research, CH-1211 Geneva 23, Switzerland.
E-mail address: irene.degl'innocenti@cern.ch (I. Degl'Innocenti).

https://doi.org/10.1016/j.nima.2020.164571
Received 14 April 2020; Received in revised form 29 July 2020; Accepted 17 August 2020
Available online 31 August 2020

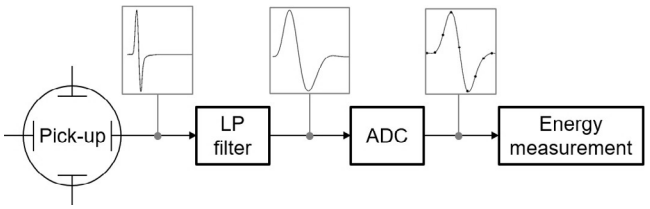

Fig. 1. Schematic representation of a BPM pick-up acquisition chain, based on direct digitization.

and distortion of the reconstructed signal for uniform, and non-uniform sampling patterns for stochastic, continuous periodic signals. They expressed bounds for the mean value and the variance of the distortion introduced by the sampling process in the reconstructed signal. Their study for periodic signals is also applicable to signals defined over a finite interval. *Kipnis, et al.* also considered the specific case of a limited bitrate budget for both uniform and non-uniform sampling for a noisy, stationary *Gaussian* random process [7]. They demonstrated that under this constraint for a process with non-uniform power density the optimal sampling frequency is below the Nyquist rate since "some distortion due to sampling is preferred in order to increase the quantizer resolution".

This result motivates the "trade-off" of selecting ADCs with lower sampling rates but higher resolution. There is a fundamental interest to analyze and better understand the lower boundary of this trade-off, and whether this can be extended through further band-limitation with the addition of a low-pass filter. A typical beam instrumentation system requires the measurement of the energy (which we sometimes call "intensity") of a series of short (ns or sub-ns time duration) pulsed signals. While the shape of the waveform is the same for each pulse, the amplitude to be measured may be different. In most applications, a low-pass pre-filtering is applied to the source signal, acting as an integrator, while also limiting the signal bandwidth, and therefore reducing the *Nyquist* sampling rate requirement (see Fig. 1). However, a filter with too low a cut-off frequency, or excessive time-domain ringing will lead to interference between consecutive pulses.

This paper presents an analysis of the effect of the finite sampling and noise introduced by the ADC, not on the distortion to the reconstructed waveform, but on the integrated signal power calculated from the individual signal samples, in order to evaluate if, and in which conditions the mean square value of a short, analog pulse is a good estimator of its total energy. The class of signals considered were deterministic, single pulse waveforms of finite energy, defined over a finite time interval, and are described formally in Section 2. The study was limited to uniform sampling, i.e., all samples taken at the same equidistant time interval. Unlike the works listed above, this analysis looks at asynchronous sampling conditions between the ADC input signal and the ADC clock for each single measurement, which applies for many practical implementations. The result of the analysis is an analytical expression for the error in the measured pulse energy introduced by sampling the analog waveform below the *Nyquist* rate (see Section 3.1). Combining this result with the effect of ADC noise, a general expression for the signal-to-noise ratio (SNR) of the measured pulse energy is obtained as a function of the pulse spectrum, the sampling frequency and the converter noise (see Section 3.2).

The error analysis method presented results in functions that can always be expressed by a limited set of discrete data values, and is therefore ideal for use in numerical simulations. The method can be applied to any arbitrary waveform, with no known analytical expression, if an oversampled numerical representation is available.

The final Section 4 presents the results of using this analysis for three typical single pulse waveforms: a *Gaussian* pulse, the derivative of a *Gaussian* pulse in the form of an analytical expression, and an oversampled numerical representation of a beam position monitor signal. All these results were verified with numerical simulations. To underline how the technology-driven ADC trade-off affects the results, the relationship between the maximum sampling frequency and the ADC resolution for commercial ADCs was taken into account. This was based on the Walden measure of performance [8], rather than the fixed bitrate budget used by *Kipnis* [7]. While the fixed bitrate budget is a popular metric in information theory to describe the limit of a communication channel, the Walden measure of performance better describes the trade-offs to be considered for state-of-the-art ADCs.

2. Problem definition

A given signal $x(t)$ to be measured has an analog, deterministic, time limited waveform, with the respective continuous spectrum $X(f)$. The quantity to be characterized by a quantitative measurement is the finite signal energy E.

$$E = \int_{-\infty}^{+\infty} |x(t)|^2 dt = \int_{-\infty}^{+\infty} |X(f)|^2 df < \infty \tag{1}$$

If the signal is limited in time, a window T can be defined such that outside this window $x(t) \approx 0$.

Such a signal can be made periodic by adding replicas of $x(t)$ spaced by nT, without altering the signal amplitude within the window T:

$$x_T(t) = \sum_{n=-\infty}^{+\infty} x(t - nT) \tag{2}$$

The spectrum of $x_T(t)$ is discrete and defined by its Fourier coefficients X_k, equivalent to the spectrum $X(f)$ sampled at multiples of $1/T$.

The power P_T of the periodic signal $x_T(t)$ can be calculated as follows:

$$P_T = \frac{1}{T}\int_0^T |x_T(t)|^2 dt = \frac{1}{T}\int_0^T |x(t)|^2 dt = \sum_{k=-\infty}^{+\infty} |X_k|^2 \tag{3}$$

Since $x(t)$ only has significant power within the window T, the energy E, Eq. (1), and the power P_T, Eq. (3), are related in the following way:

$$E = \int_{-\infty}^{+\infty} |x(t)|^2 dt = \int_0^T |x(t)|^2 dt = T \cdot P_T \tag{4}$$

To determine the energy it is therefore sufficient to determine the power of $x(t)$ within T, Eq. (3).

Let us assume the signal $x_T(t)$ is sampled with an infinite resolution with respect to the reported amplitudes. The sampling frequency F_s is related to the window length T, which needs to be an integer multiple of the sampling period $t_s = 1/F_s$. This fact does not limit the choice of sampling frequency, as the window length can always be increased with respect to the minimum length T that satisfies $x(t) \approx 0 \; \forall \; t > T$. The discrete sequence $\hat{x}_n$ is the result of the sampling process, and $N = F_s T$ gives the number of samples within the window T. The associated Discrete *Fourier* Transform (DFT)[1] is the sequence $\hat{X}_k$ of N complex coefficients.

The power of the sampled signal sequence of period T is then given as:

$$\hat{P}_T = \frac{1}{N}\sum_{n=0}^{N-1} \hat{x}_n^2 \tag{6}$$

Some questions now have to be discussed:

1. Under which conditions is $\hat{P}_T$ a good estimator of P_T?
2. If a variation of the sampling phase is imposed on the sequence $\hat{x}_n$, what effect does it have on $\hat{P}_T$?

[1] The definition of the DFT used in the present work is the following:

$$x_n = \sum_{k=0}^{N-1} X_k \exp(j2\pi k \frac{n}{N}) \iff X_k = \frac{1}{N}\sum_{n=0}^{N-1} x_n \exp(-j2\pi k \frac{n}{N}) \tag{5}$$

3. What is the mean value and the variance of the error of the power calculation if the signal considered is not noiseless?

Questions 1 and 2 are discussed in 3.1, while question 3 is discussed in 3.2.

3. General results

In this section, starting from the model described in the previous Section 2, we analyze the effects of sampling distortion and noise on the calculation of the pulse power, and hence energy, within the window T. This leads to an expression for the signal-to-noise ratio of the power measurement as a function of the signal spectrum, sampling frequency and total noise.

3.1. Error of the power calculation for a noiseless pulsed signal caused by sampling distortion

The signal power within the time window T, as shown in Eq. (3), can be calculated in both time and frequency domain. As the power P_T is limited, the series $|X_k|^2$ converges. We always assume our pulsed signal to be bandlimited, with *Fourier* coefficients vanishing above the harmonic N_0:

$$|X_i|^2 = 0 \qquad \forall\, i \;:\; |i| > N_0 \tag{7}$$

which allows the following equation:

$$P_T = \sum_{k=-\infty}^{+\infty} |X_k|^2 = \sum_{k=-N_0}^{+N_0} |X_k|^2 \tag{8}$$

It is worth noticing that the coefficients X_k, cut off at the frequency N_0/T, are the result of the Discrete *Fourier* Transform of the periodic signal $x_T(t)$, sampled with a frequency $F_s = 2N_0/T$. As a consequence, the signal power within the window T can be determined without significant loss of information by a limited set of *Fourier* coefficients X_k, with this limited set of coefficients calculated analytically from the time-domain expression of the signal by a *Fourier* transform. These coefficients can also be obtained numerically, via the Discrete *Fourier* Transform of an oversampled numerical representation of the time-domain waveform within the window T, requiring at least $2N_0$ samples. The following steps, focusing on the error in determining the signal power assuming undersampling, can therefore equally well be applied to any arbitrary waveform through oversampling.

The time sequence $\hat{x}_n$ of N samples, as a result of sampling $x_T(t)$ within T at an arbitrary frequency $F_s = N/T$, was defined in Section 2, together with the signal power estimator $\hat{P}_T$ (6). Applying the *Parseval*'s theorem for the Discrete *Fourier* Transform, the power estimator $\hat{P}_T$ can also be expressed as a function of the DFT coefficients $\hat{X}_k$ of the sampled sequence:

$$\hat{P}_T = \sum_{k=0}^{N-1} |\hat{X}_k|^2 \tag{9}$$

Furthermore, the sequence $\hat{X}_k$ can be expressed as a function of X_k, which are the *Fourier* coefficients of the continuous periodic signal $x_T(t)$, as $\hat{x}_n$ is obtained by sampling $x_T(t)$. $\hat{X}_k$ result from making the coefficients X_k periodic, and can be constructed from a series of overlapping replicas of the spectrum coefficients X_k, shifted by integer multiples of the sampling frequency F_s.

$$\hat{X}_k = \sum_{m=-\infty}^{+\infty} X_{k+mN}, \qquad k = 0, 1, \dots, N-1 \tag{10}$$

Assuming a band-limited signal (Eq. (7)), and $F_s > 2N_0/T = R_{Nyq}$, i.e., $N > 2N_0$, the *Nyquist–Shannon* criterion is respected since the sampling frequency is higher than the *Nyquist* rate, and the expression (10) can be simplified to:

$$\hat{X}_k = \begin{cases} X_k, & \text{if} \quad k = 0, 1, \dots, \lfloor N/2 \rfloor \\ X_{k-N}, & \text{if} \quad k = \lfloor N/2 \rfloor + 1, \dots, N-1 \end{cases}$$

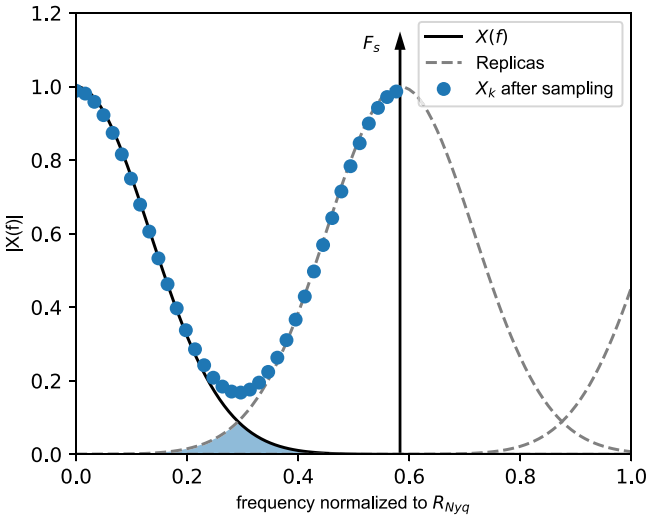

Fig. 2. Aliasing of the first replica of a *Gaussian* spectrum for sampling at ∼ 0.59 of the *Nyquist* rate.

Under these conditions the sampling process does not introduce errors, and $\hat{P}_T$ is therefore a good estimator of P_T:

$$\hat{P}_T = \sum_{k=0}^{N-1} |\hat{X}_k|^2 = \sum_{l=-\lfloor N/2 \rfloor}^{\lfloor N/2 \rfloor} |X_l|^2 = \sum_{l=-N_0}^{N_0} |X_l|^2 = P_T \tag{11}$$

where $l = k - \lfloor N/2 \rfloor$.

The situation is different when oversampling is not achieved, i.e., $N < 2N_0$ and $F_s < R_{Nyq}$. In this case, the coefficients $\hat{X}_k$ of the DFT are affected by aliasing. Let us assume $N > N_0$, i.e., $F_s > R_{Nyq}/2$, then only the first shifted replica of $X(f)$ will affect the sequence (see Fig. 2), and the coefficients $\hat{X}_k$ for $k = 0, 1, \dots, N-1$ can be expressed as:

$$\hat{X}_k = X_{k-N} + X_k \tag{12}$$

To see how $\hat{P}_T$ is affected, the square of the absolute value of $\hat{X}_k$ for $k = 0, 1, \dots, N-1$ is expressed as a function of the coefficients $X_k = |X_k| \exp(j\phi_k)$:

$$|\hat{X}_k|^2 = |X_k|^2 + |X_{k-N}|^2 + 2|X_k||X_{k-N}| \cdot \cos(\phi_k - \phi_{k-N}) \tag{13}$$

The power of the sequence, $\hat{P}_T$, is now expressed as:

$$\hat{P}_T = \sum_{k=-N}^{N-1} |X_k|^2 + \sum_{k=0}^{N-1} 2|X_k||X_{k-N}| \cdot \cos(\phi_k - \phi_{k-N}) \tag{14}$$

Under the hypothesis $N > N_0$, the first sum of Eq. (14) is P_T, Eq. (8), while the second sum expresses the error introduced by undersampling. This error depends on the power spectral density of the pulse and on the phase of the spectral coefficients.

Let us consider the case where the periodic, pulsed signal $x_T(t)$ is sampled with a different sampling phase, expressed by a time delay τ. The resulting sequence $\hat{x}_{n,\tau}$, with the respective DFT coefficients $\hat{X}_{k,\tau}$, is then defined by:

$$\hat{x}_{n,\tau} = x_T(nt_s - \tau), \qquad n = 0, 1, \dots, N-1 \tag{15}$$

In the case where $N_0 < N < 2N_0$, i.e., $R_{Nyq}/2 < F_s < R_{Nyq}$, leading to aliasing of the first replica, the coefficients $\hat{X}_{k,\tau}$ can be found directly from (12):

$$\hat{X}_{k,\tau} = X_{k-N} \cdot \exp\left(-j2\pi(k-N)\frac{\tau}{T}\right) + X_k \cdot \exp\left(-j2\pi k \frac{\tau}{T}\right), \quad k = 0, 1, \dots, N-1 \tag{16}$$

The square of the absolute value of the coefficients follows as:

$$|\hat{X}_{k,\tau}|^2 = |X_k|^2 + |X_{k-N}|^2 + 2|X_k||X_{k-N}| \cdot \cos\left(\phi_k - \phi_{k-N} - 2\pi N \frac{\tau}{T}\right) \tag{17}$$

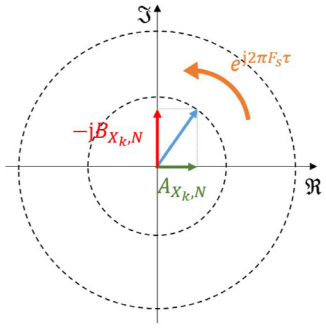

Fig. 3. Complex phasor showing the power measurement error caused by sampling a repetitive pulsed signal with a fixed delay τ.

The result is similar to (13), but with an additional term in the argument of the cosine. The power estimator now also includes the dependency of the error due to the sampling delay:

$$\hat{P}_{T,\tau} = P_T + 2\sum_{k=0}^{N-1} |X_k||X_{k-N}| \cdot \cos\left(\phi_k - \phi_{k-N} - 2\pi F_s \tau\right) \tag{18}$$

The power measurement error is defined as $\epsilon_{P_{T,\tau}} \doteq \hat{P}_{T,\tau} - P_T$, and can be expressed as (see Appendix A.1 for details):

$$\epsilon_{P_{T,\tau}} = A_{X_k,N} \cdot 2\cos(2\pi F_s \tau) + B_{X_k,N} \cdot 2\sin(2\pi F_s \tau) \tag{19}$$

with:

$$\begin{aligned} A_{X_k,N} &\doteq \sum_{k=0}^{N-1} |X_k||X_{k-N}| \cdot \cos(\phi_k - \phi_{k-N}) \\ B_{X_k,N} &\doteq \sum_{k=0}^{N-1} |X_k||X_{k-N}| \cdot \sin(\phi_k - \phi_{k-N}) \end{aligned} \tag{20}$$

This error $\epsilon_{P_{T,\tau}}$ can be rewritten as:

$$\epsilon_{P_{T,\tau}} = 2\Re\left((A_{X_k,N} - jB_{X_k,N})\exp(j2\pi F_s \tau)\right) \tag{21}$$

It can be visualized as the projection of twice the length of a phasor on the real axis, whose modulus depends on the coefficients of the signal spectrum, and whose phase depends on the sampling frequency and delay (see Fig. 3). If the phase rotation, i.e., the sampling delay, is distributed uniformly, we can expect the mean value of the error for multiple measurements to be zero. However if the sampling phase is locked to the signal, the error on the power measurement remains constant with an absolute value within the range $\left[0, 2\sqrt{A^2_{X_k,N} + B^2_{X_k,N}}\right]$.

The sampling delay τ, caused by an asynchronous sampling phase, can be modeled as a random variable described by a probability density function. Let us assume τ to be a continuous uniform random variable, defined in the interval between zero and sampling period $t_s = T/N$ ($\tau = \mathrm{U}[0, t_s]$). The mean μ_ϵ and variance σ^2_ϵ of the power measurement error, $\epsilon_{P_{T,\tau}}$, are given by (see Appendix A.2):

$$\mu_\epsilon = \mathrm{E}[\epsilon_{P_{T,\tau}}] = 0 \tag{22}$$

$$\sigma^2_\epsilon = \mathrm{E}[(\epsilon_{P_{T,\tau}} - \mu_\epsilon)^2] = 2(A^2_{X_k,N} + B^2_{X_k,N}) \tag{23}$$

From (22) it follows that $\hat{P}_{T,\tau}$ is an unbiased estimator for P_T, for a noiseless signal and a uniformly distributed sampling phase. On the other hand, the variance of the error depends on both the signal spectrum and the sampling frequency.

Since the error $\epsilon_{P_{T,\tau}}$ is expressed as an analytical function of a random variable whose probability density function is known, we can also calculate the probability density function of the error to have further insights about the sampling error behavior (see Appendix A.3). It is note-worthy that the error probability is higher for large errors, within the limits given by the range of possible error values. Fig. 4 shows as example the probability density function for a *Gaussian* pulse signal, as described in Section 4.1. This distribution must be taken into account when designing systems using asynchronously sampled data.

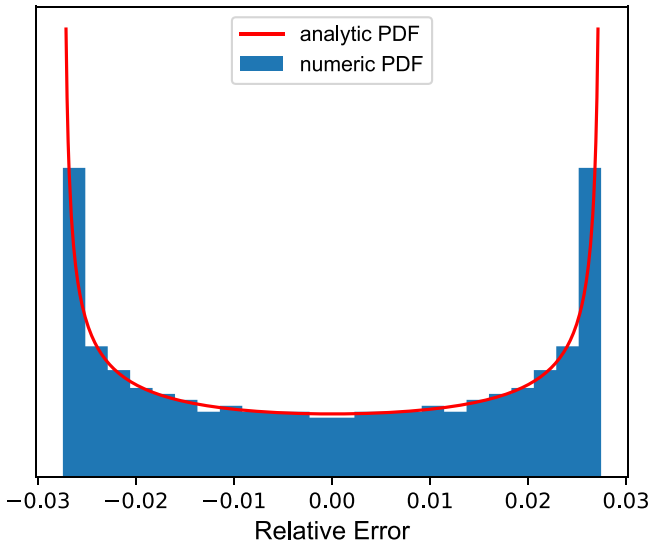

Fig. 4. Probability Density Function (PDF) of the relative error of the power measurement of a *Gaussian* pulse signal (as described in Section 4.1), when sampled at half of its *Nyquist* rate (analytical and numerical result).

3.2. Introduction of Gaussian noise and SNR analysis

A noisy system is typically analyzed by modeling the comprehensive noise, e.g., as a zero-mean *Gaussian* variable ν_i, with variance σ^2_ν, added to the otherwise noiseless signal. This noise contribution is propagated to the power measurement when performing the mean square of the sampled sequence. The estimated power including the noise contribution is then given by $\bar{P}_T$:

$$\bar{P}_T = \frac{1}{N}\sum_{n=0}^{N-1}\left(\hat{x}_n + \nu_n\right)^2 = \hat{P}_T + \frac{1}{N}\sum_{n=0}^{N-1}\nu_n^2 + \frac{1}{N}\sum_{n=0}^{N-1} 2\hat{x}_n\nu_n \tag{24}$$

Let us define the random variable $\eta\left(P_T, \sigma^2_\nu, N\right) \doteq \bar{P}_T - \hat{P}_T$, which expresses the contribution to the error by the noise injected into the system. This error η is a function of the signal power, the noise variance and the sampling frequency. Its mean value μ_η and its variance σ^2_η are calculated as (Appendix B):

$$\mu_\eta = \sigma^2_\nu \tag{25}$$

$$\begin{aligned} \sigma^2_\eta &= 2\frac{\sigma^4_\nu}{N} + 4\frac{\sigma^2_\nu}{N^2}\sum_{n=0}^{N-1}\left(\mathrm{Var}\left[\hat{x}_n\right] + \mathrm{E}\left[\hat{x}_n\right]^2\right) \\ &\simeq 2\frac{\sigma^4_\nu}{N} + 4\frac{\sigma^2_\nu}{N}P_T \end{aligned} \tag{26}$$

Summing both the sampling error ϵ and the noise error η to the power measurement gives:

$$\bar{P}_T = P_T + \epsilon\left(X_k, N, \tau\right) + \eta\left(P_T, \sigma^2_\nu, N\right) \tag{27}$$

Both of these contributions are known in terms of their mean value and variance.

The mean value of the total error is equal to the mean of the noise error (25) as the mean of the sampling error is zero.

To calculate the variance of the total error, the relationship between these two errors must be considered. For high sampling rates it is reasonable to assume that the dependence of the noise error on changes in the sampling phase is negligible (see the conclusions of Appendix B),

so that the noise error variance can be approximated as in (26). The two errors are thus considered independent and the total error variance simply becomes the sum of the two individual variances.

From a system design perspective, it is useful to combine the results in the form of a SNR expression. In most cases, the engineer is interested in guaranteeing some minimum SNR. Using such an expression it is therefore possible to navigate the ADC specification space to find a solution that fulfills this requirement for given input signal conditions. The signal-to-noise ratio expression also shows how the various error terms limit the final pulse energy measurement:

$$SNR_{dB} = 10\log_{10}\left(\frac{P_T^2}{\sigma_\epsilon^2+\sigma_\eta^2}\right) = 10\log_{10}\left(\frac{P_T^2}{2(A_{X_k,N}^2+B_{X_k,N}^2)+2\frac{\sigma_v^4}{N}+4\frac{\sigma_v^2}{N}P_T}\right) \quad (28)$$

with $A_{X_k,N}$ and $B_{X_k,N}$ as defined in (20).

4. Application to example waveforms and remarks on ADC parameter trade-offs

The general result of the analysis presented above were applied to four different deterministic waveforms:

- a *Gaussian* waveform;
- the derivative of a *Gaussian* waveform;
- the analytical expression for the waveform obtained from the response of a LHC stripline beam position monitor pick-up to a charged particle bunch;
- the measurement from an oscilloscope of the response of a LHC stripline beam position monitor pick-up to a charged particle bunch.

The *Gaussian* waveform and the derivative of the *Gaussian* waveform are generic signals that fit practical distributions. In beam diagnostic, for example, a beam current transformer signal can be approximated with a *Gaussian* waveform. On the other hand, the derivative of a *Gaussian* waveform approximates the response of differential capacitive systems, as button and stripline pickups in a particle accelerator. The LHC stripline beam position monitor is here used as a specific example.

In an actual instrument these signals would require some pre-processing before digitization, depending on the signal itself and on the measurement requirements in terms of performance and bandwidth. Here, pre-filtering and sources of perturbation other than the ADC are omitted for the sake of generality, and to keep the signals defined by analytical expressions, enabling the reader to easily reproduce them.

Closed, analytic formulae for the total pulse energy error and for the SNR are provided for the *Gaussian* pulse, whilst for the other cases the energy error and the SNR are expressed as a function of the signal spectrum, obtained by numerical calculation of a Fast *Fourier* Transformation (FFT) of the oversampled waveform, limited to a time window T.

These signal examples and the digitization parameters used fit the hypotheses assumed in the previous sections, namely:

- the signal has finite energy and is limited in time;
- the sampling frequency is in the range $R_{Nyq}/2 < F_s < R_{Nyq}$ and therefore only the aliasing of the first replica is relevant;
- the sampling phase is a uniformly distributed random variable;
- the noise is described by an independent and identically distributed, zero-mean, *Gaussian* variable.

For all examples the analytical, or quasi-analytical "oversampled" results have been compared with numerical simulations. The variation in pulse energy error was calculated after sampling the input signal with a uniformly distributed sampling delay, and by adding *Gaussian* noise. While the examples of a *Gaussian* pulse and derivative of a *Gaussian* pulse are expressed in normalized time and frequency coordinates, the BPM related examples use the actual time window and sampling frequencies consistent with the oscilloscope-based measurement. This allowed the ADC noise to be expressed as a function of the sampling frequency, referring to commercially available, state-of-the-art ADCs. Using this approach it was then possible to find a good compromise between the maximum sampling frequency and the resolution of the ADC, to maximize the SNR for a specific input signal.

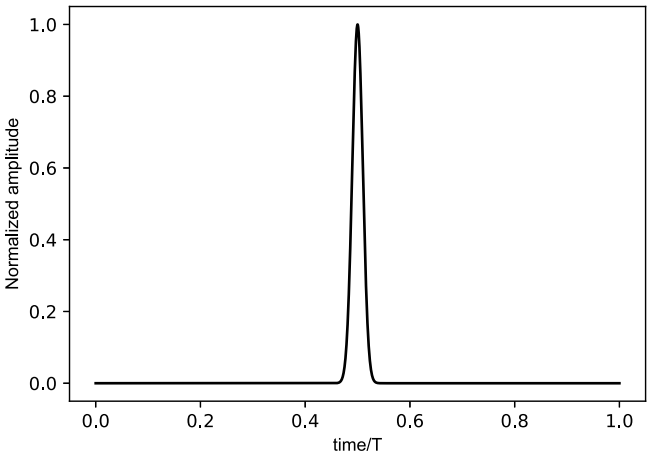

Fig. 5. *Gaussian* waveform in the time domain.

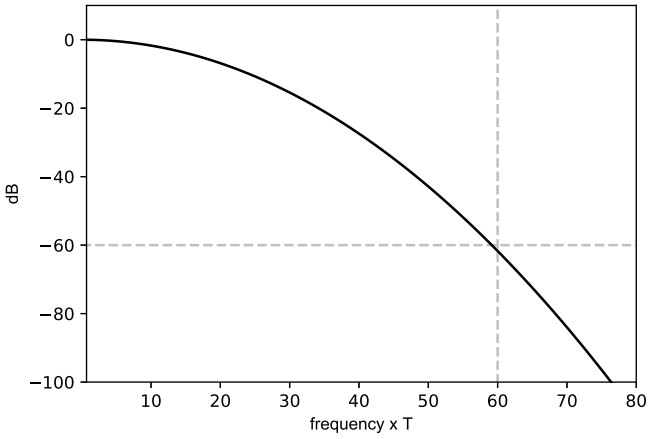

Fig. 6. *Gaussian* waveform in the frequency domain, indicating the chosen bandwidth limit at −60 dB.

4.1. Gaussian waveform and derivative of a Gaussian waveform

A *Gaussian* waveform with standard deviation σ and its maximum amplitude in the center of time window T is given by:

$$x(t) = \frac{1}{\sqrt{2\pi\sigma^2}}\exp\left(-\frac{(t-T/2)^2}{2\sigma^2}\right) \quad (29)$$

Setting $\sigma = 0.01T$ the pulse width with respect to the window size is comparable to the one of the BPM example (see 4.2) and the signal can be considered to be zero outside this window.

The result of the *Fourier* transformation of (29) follows as:

$$X(f) = \exp(-2\pi^2\sigma^2 f^2)\exp(-j2\pi fT/2) \quad (30)$$

The signal $x(t)$ and the modulus of its spectrum $|X(f)|$ are shown in Figs. 5 and 6 respectively (the latter with logarithmic scaling). The

signal pulse has a finite energy E given by:

$$E = \int_{-\infty}^{+\infty} x(t)^2 dt = \frac{1}{2\sqrt{\pi\sigma^2}} \tag{31}$$

Using the periodic form of (29) over the period T, and following (4), the discrete spectrum X_k is the sampled version of $X(f)$ at multiples of $1/T$:

$$X_k = X\left(\frac{k}{T}\right) = \exp(-2\pi^2 \frac{\sigma^2}{T^2} k^2)\exp(-j\pi k) \tag{32}$$

To locate the range of sampling frequencies for which the energy error expression is valid, the bandwidth, i.e., the parameter N_0 of (7), must be defined. The *Fourier* transformation of a *Gaussian* function is itself a *Gaussian* function, therefore the power density $|X(f)|^2 \neq 0 \; \forall \; f$. However, a threshold can be set below which the spectral power can be considered negligible. In this example the threshold was set to $|X_k|_{\text{dB}} \leq -60$ dB, for a spectrum normalized with respect to its maximum value. The value -60 dB $\equiv 10^{-3}$ is rather arbitrarily chosen for this example, but is compatible with the typical noise level of commercial ADCs being investigated for this particular application [9–13]. In any practical application this bandwidth limit must be set coherently with the expected noise level. Verifying the bandwidth condition for $k \geq 60$, gives $N_0 = 60$ and a *Nyquist* rate of $R_{Nyq} = 2N_0/T = 120/T$.

At this point, all elements to express the error due to asynchronous sampling in the range $R_{Nyq}/2 < F_s < R_{Nyq}$ are given. The coefficients $A_{X_k,N}$ and $B_{X_k,N}$ (definition (20)) follow as:

$$\begin{aligned} A_{X_k,N} &= (-1)^N \exp(-2\pi^2 \frac{\sigma^2}{T^2} N^2) \sum_{k=0}^{N-1} \exp(4\pi^2 \frac{\sigma^2}{T^2} k(N-k)) \\ B_{X_k,N} &= 0 \end{aligned} \tag{33}$$

and the variance of the error due to asynchronous sampling is given by:

$$\sigma_\epsilon^2 = 2A_{X_k,N}^2 = 2\left[\exp(-2\pi^2 \frac{\sigma^2}{T^2} N^2) \sum_{k=0}^{N-1} \exp(4\pi^2 \frac{\sigma^2}{T^2} k(N-k))\right]^2 \tag{34}$$

For the full picture, the noise related to the ADC also needs to be included. This is described by the variance σ_v^2, and leads to an error variance contribution following (26). Referring to the definition of Effective Number Of Bits (ENOB), we can express the standard deviation of the noise of the ADC as:

$$\sigma_v = \frac{V_{FSR}}{\sqrt{12}} 2^{-\text{ENOB}} \tag{35}$$

where V_{FSR} is the full-scale range of the ADC input signal. For our example V_{FSR} was set to twice the maximum absolute value of the input signal to take into account bipolar waveforms.

Fig. 7 shows the result for the *Gaussian* waveform (29) as SNR vs. F_s/R_{Nyq}, i.e., (28), with (34) for the sampling distortion contribution to the error, and for two values of σ_v reflecting the ADC noise contribution to the error. In one case the standard deviation σ_v is set to a value of -70 dB $\equiv 3.16 \cdot 10^{-4}$ with respect to the full-scale-range (maximum) input signal value of the ADC, equivalent to a 11.33 ENOB ADC. In the other case the ADC noise contribution is doubled, with σ_v set to a value of -64 dB $\equiv 6.3 \cdot 10^{-4}$. This is equivalent to the noise of a 10.33 ENOB ADC. The plot shows the SNR as a function of the total error, combining the two error sources. It also shows the SNR when only one source of error, either sampling or noise, is taken into account. The results from the analytical computation are observed to be confirmed by numerical analysis.

Fig. 7 can be split into three regions: at low sampling frequencies the achievable SNR is dominated by the effect of sampling distortion; at high sampling frequencies the SNR is limited by the noise of the ADC; between these two regions is a rather narrow transition region, with the frequency at which this transition happens depending on the noise. The less noisy the ADC the higher the transition frequency and the more we can increase the signal to noise ratio through using higher sampling rates.

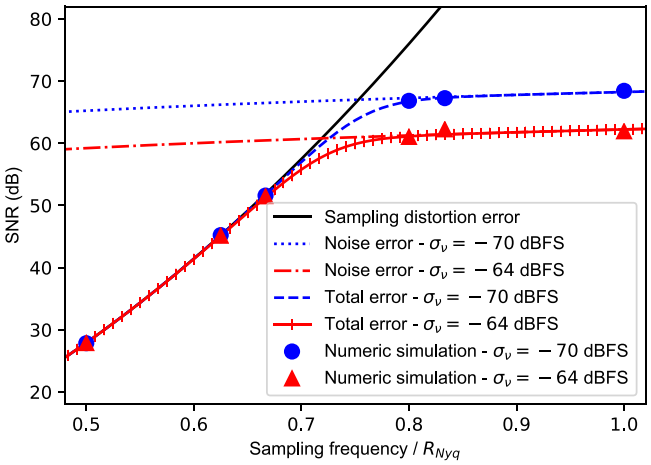

Fig. 7. SNR as function of the normalized sampling rate for a *Gaussian* waveform.

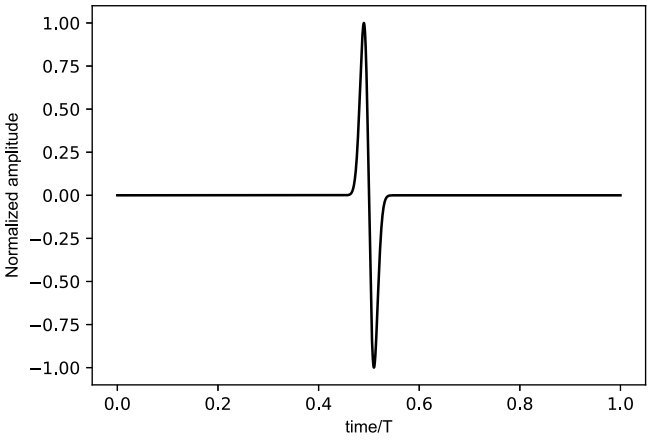

Fig. 8. Derivative of a *Gaussian* pulse in the time domain.

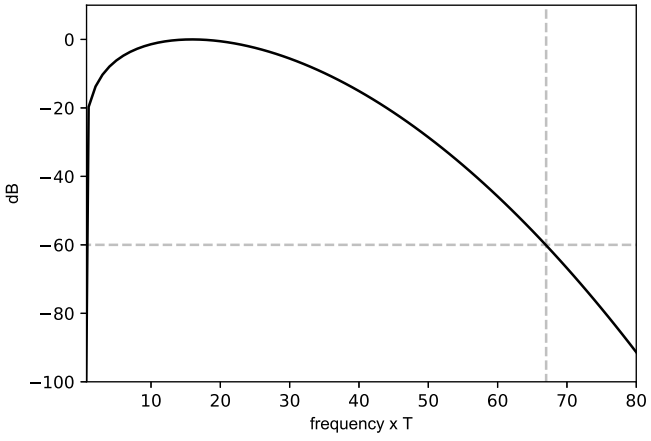

Fig. 9. Derivative of a *Gaussian* pulse in the frequency domain, indicating the bandwidth limit at −60 dB.

The derivative of the *Gaussian* pulse was chosen as an example of a bipolar pulse, as it closely resembles the type of signal produced by many electromagnetic pick-ups in particle accelerators. The time domain signal and frequency domain spectrum are shown in Figs. 8 and 9 respectively (the latter with logarithmic scaling). The same

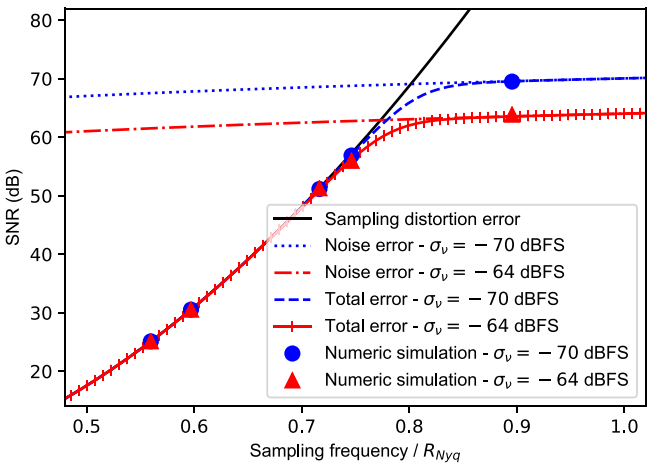

Fig. 10. SNR as function of the normalized sampling rate for a differentiated *Gaussian* waveform.

formalism was applied to this signal as for the *Gaussian* signal pulse, except that the discrete spectrum X_k was not obtained by sampling the analytically calculated spectrum $X(f)$, but numerically from an FFT on an oversampled sequence of the time-domain waveform. Fig. 10 shows the SNR results in the same format as Fig. 7, and for the same noise contribution values of σ_v. Again, a good match is observed with respect to the values obtained through numerical analysis. This confirms the validity of this approach also for the analysis of bipolar signals.

4.2. Typical beam position monitor signals, analytical expression and oscilloscope measurement

The beam position monitor (BPM) is an electromagnetic transducer which delivers a pulsed output signal as it is excited by a passing bunch of charged particles. While there are different types of BPMs [1], we consider here the directional coupler BPM as an example, and use for reference the geometry and dimensions of a typical directional coupler BPM installed in the Large Hadron Collider (LHC) at CERN.

A directional coupler BPM consists of two or four orthogonally oriented coupling electrodes. Each electrode can be considered to be a transmission-line with a characteristic impedance Z_0. The electrodes are often shaped as strip transmission-lines with $Z_0 = 50\ \Omega$, and this is the reason why this type of directional coupler BPM is sometimes known as a "stripline BPM". An ideal directional coupler electrode will only sense the incoming beam at its upstream port. A dual port electrode can therefore be used to distinguish the beam direction, but this is not of relevance for the following discussion, where we limit the discussion to a single charged particle bunch passing the electrode in one direction.

Consider a relativistic beam, i.e., with a velocity close to the speed of light, with a *Gaussian* shaped longitudinal bunch profile similar to (29), passing the BPM at the center, along the line of transverse symmetry. The upstream port of each stripline electrode will generate a voltage pulse given by [1]:

$$V_{up}(t) = \frac{\phi}{2\pi}\frac{Z_0}{2}\frac{eN_b}{\sqrt{2\pi}\sigma_t}\left[\exp\left(-\frac{(t+t_{\ell'})^2}{2\sigma_t^2}\right) - \exp\left(-\frac{(t-t_{\ell'})^2}{2\sigma_t^2}\right)\right] \tag{36}$$

The definition of each parameter of (36) and their value for the LHC stripline BPM case are listed in Table 1.

Fig. 11 shows the signal according to (36) for a time window of $T = 24$ ns, contained within the LHC bunch spacing of 25 ns. The frequency spectrum is shown in Fig. 12. Applying our bandwidth limit at −60 dB below maximum magnitude gives corresponding frequency of 2.21 GHz, which results in a *Nyquist* rate of 4.42 GHz. As for the previous example of the *Gaussian* derivative, the spectral coefficients

Table 1
Definition and value of the parameters of the LHC stripline BPM bunch response expression.

Symbol	Definition	Value
Z_0	Port impedance	50 Ω
$t_{\ell'}$	Propagation delay	417 ps
ϕ	Electrode azimuthal width	0.27 rad
e	Elementary charge	$1.602 \cdot 10^{-19}$ C
N_b	Bunch intensity	10^{10}
σ_t	Bunch length	0.25 ns

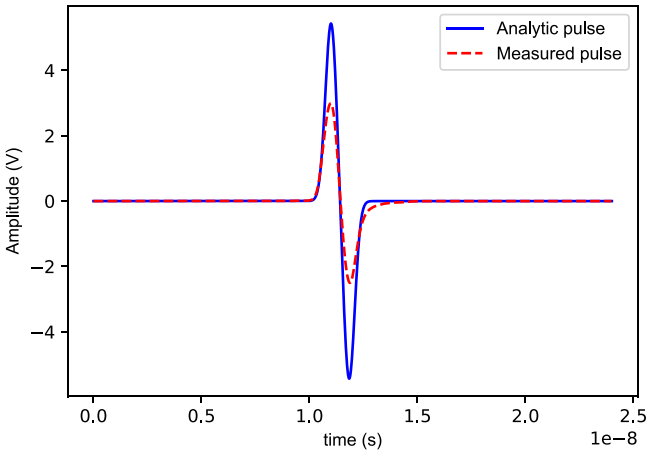

Fig. 11. Analytic signal and measured signal using a broadband oscilloscope for a charged particle bunch detected by a directional coupler BPM, in the time domain.

X_k are computed numerically using an FFT. As our method can be used for any oversampled numerical signal waveform, this analytic signal can be compared to an actual bunch signal from an LHC directional coupler BPM pickup acquired by a broadband, fast sampling (60 GS/s) oscilloscope. The measured signal waveform is also shown in Fig. 11, normalized to the same $N_b = 10^{10}$ bunch intensity, with the corresponding frequency domain spectrum shown in Fig. 12. Again, setting the bandwidth limit to −60 dB results in a cut-off frequency of 2.67 GHz, with the associated *Nyquist* rate of 5.34 GHz. The longitudinal particle dynamics in the LHC is complex, it cannot be simply approximated by a *Gaussian* distribution function. A real BPM stripline has inevitable complexities and imperfections, as well. That is why the measured bunch BPM signal appears to have more spectral content at high frequencies with respect to the analytical approximation.

For this example, an ADC should be investigated in the range of sampling frequencies $2.21 < F_s < 4.42$ GHz for the analytical signal and in the range of sampling frequencies $2.67 < F_s < 5.34$ GHz for the measured signal, corresponding to $R_{Nyq}/2 < F_s < R_{Nyq}$ for the two cases. Instead of assuming a constant noise contribution of the ADC, as in Section 4.1, we rely on data from commercially available ADC products for this range of F_s, and associate a realistic resolution with each sampling frequency.

In his ADC survey [8] Walden collected data about the distribution of resolution versus sampling rate of state-of-the-art converters. He observed that, for high sampling rates, "approximately one bit of resolution is lost for every doubling of the sampling rate". This information can be summarized in the universal measure of ADC performance that he named P, defined as the effective number of quantization levels times the sampling rate:

$$P \doteq 2^{\mathrm{ENOB}} F_s \tag{37}$$

This product has improved over time for every new generation of ADC chips, with technology advancements achieving higher resolution at higher sampling rates.

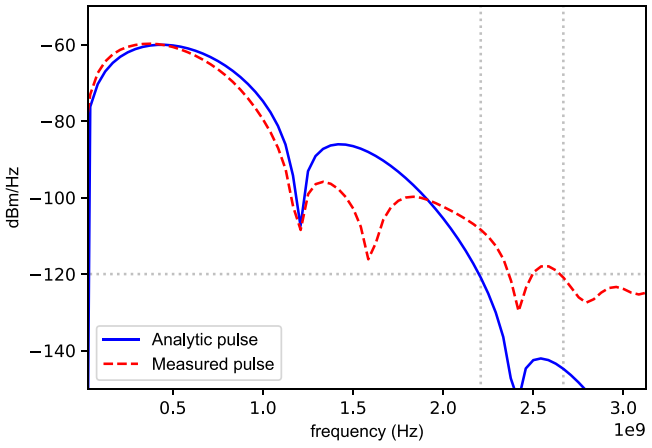

Fig. 12. Analytic signal in the frequency domain and frequency domain representation of a measured signal using a broadband oscilloscope (power spectral density normalized to the total integrated average power, showing the imposed bandwidth limit at −60 dB with respect to the peak) for a charged particle bunch detected by a directional coupler BPM.

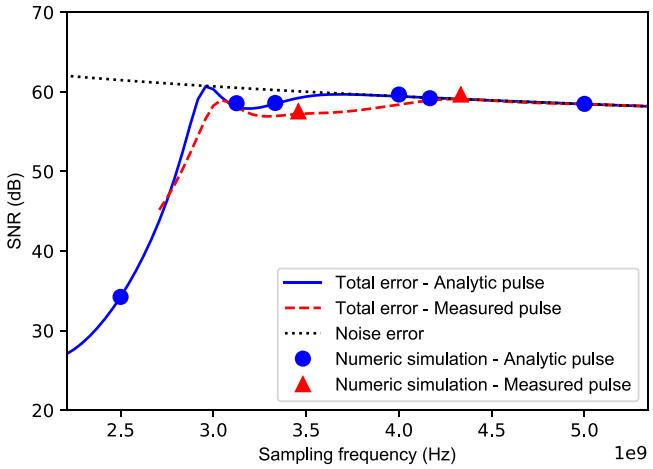

Fig. 13. SNR of the pulse energy measurement as function of the ADC sampling frequency for a charged particle bunch detected by a directional coupler BPM.

Investigating the data-sheets of commercially available ADC chips with sampling rates in our range of interest [9–13], an average value of $P = 2.3 \cdot 10^{12}\ \mathrm{s}^{-1}$ was found.

By combining the expression (35) and the definition (37), we can express the standard deviation of the noise of the ADC as a function of the sampling rate:

$$\sigma_v = \frac{V_{FSR}}{\sqrt{12}} \frac{F_s}{P} \tag{38}$$

Again, in this example the full scale range for the ADC input signal (V_{FSR}) was set to twice the maximum absolute value of the input signal.

Fig. 13 displays the result of the SNR computation for the energy estimation of both the analytic and measured BPM signals, taking into account both sampling distortion error and the ADC noise, with the latter now dependent on the sampling rate. The solid points show the results of the numerical analyses, which are again in good agreement with the analytical SNR results. The effect solely due to the noise of the ADC is represented separately. In comparison to the noise calculation for the *Gaussian* and differentiated *Gaussian* pulses, where the ADC noise was assumed to be constant with respect to the sampling frequency, the SNR in this case decreases at higher sampling rates, as the noise increases due to the lower effective ADC resolution.

Combining the noise effects with sampling distortion effects, leads to a transition region at lower F_s than observed for the *Gaussian* and differentiated *Gaussian* pulses, where the ADC properties were kept constant with sampling frequency (Figs. 7 and 10). This transition now occurs at smaller fractions of the Nyquist rate, compared to the case with constant ADC parameters, with the ADC noise starting to dominate at lower frequencies. The transition region is also narrower, as a consequence of the ADC noise error contribution worsening with higher sampling rates, instead of decreasing, as in the case with constant ADC noise.

Fig. 13 therefore allows us to find the optimal trade-off between sampling rate and ADC resolution for the best achievable SNR performance when measuring the pulse energy.

5. Conclusions

The analysis method presented in this paper allows calculation of the Signal to Noise Ratio (SNR) when measuring the energy content of an arbitrary, time limited waveform, considering the sampling frequency and effective resolution of the ADC used. It can serve as a powerful design tool to optimize the ADC choice for achieving the minimum error on the measurement of the energy content of a pulsed signal. Two distinct regimes are observed, one at lower frequencies where the SNR of the energy measurement is limited by the effect of sampling distortion, and one at high frequencies where the error is dominated by the ADC noise. The exact transition frequency between these two regimes depends on the bandwidth of the input signal and the associated ADC choice. The optimum sampling frequency is observed to lie well below the Nyquist rate when taking into account realistic ADC parameters for the frequency regime discussed in this paper. Although discussed in the context of measurement of beam position for particle accelerators the method has applicability for any technique relying on measuring the energy content of pulsed waveforms. This analysis is based on the relationship between the power calculated in time and frequency domain, starting with the expression of the signal spectrum as a discrete and finite sequence. This gives the method a lot of flexibility, allowing it to be applied to any pulsed waveform, described either as an analytical function or in an oversampled numerical form from a computation or a measurement. As all the analytical calculations only involve manipulation of a finite number of coefficients, the analysis can be easily implemented in any numeric environment.

CRediT authorship contribution statement

Irene Degl'Innocenti: Conceptualization, Methodology, Software, Writing - original draft. **Andrea Boccardi:** Conceptualization, Methodology, Writing - reviewing and editing, Supervision. **Luca Fanucci:** Writing - review and editing, Supervision. **Manfred Wendt:** Conceptualization, Writing - review and editing, Supervision.

Declaration of competing interest

The authors declare that they have no known competing financial interests or personal relationships that could have appeared to influence the work reported in this paper.

Appendix A. Proofs of sampling distortion error analysis

A.1. Proof of expression (19)

The sampling distortion error term $\epsilon_{P_{T,\tau}}$ appears in Eq. (18) in the form:

$$\epsilon_{P_{T,\tau}} = 2 \sum_{k=0}^{N-1} |X_k||X_{k-N}| \cdot \cos\left(\phi_k - \phi_{k-N} - 2\pi F_s \tau\right) \tag{A.1}$$

Remembering that $\cos(a-b) = \cos a \cos b + \sin a \sin b$, the cosine term in the sum can be split:

$$\cos\left(\phi_k - \phi_{k-N} - 2\pi F_s \tau\right) = \cos(\phi_k - \phi_{k-N})\cos(2\pi F_s \tau) + \sin(\phi_k - \phi_{k-N})\sin(2\pi F_s \tau) \tag{A.2}$$

The sampling distortion error term $\epsilon_{P_{T,\tau}}$ can then be rewritten as:

$$\epsilon_{P_{T,\tau}} = 2\cos(2\pi F_s \tau) \sum_{k=0}^{N-1} |X_k||X_{k-N}| \cdot \cos(\phi_k - \phi_{k-N}) + 2\sin(2\pi F_s \tau) \sum_{k=0}^{N-1} |X_k||X_{k-N}| \cdot \sin(\phi_k - \phi_{k-N}) \tag{A.3}$$

The arguments of the two series are now deterministic function of the signal spectrum and of the sampling frequency. To get a more synthetic expression, the following coefficients are defined:

$$A_{X_k,N} \doteq \sum_{k=0}^{N-1} |X_k||X_{k-N}| \cdot \cos(\phi_k - \phi_{k-N})$$
$$B_{X_k,N} \doteq \sum_{k=0}^{N-1} |X_k||X_{k-N}| \cdot \sin(\phi_k - \phi_{k-N}) \tag{A.4}$$

A.2. Computation of sampling distortion error mean and variance

The sampling delay τ is a continuous uniform random variable defined in the interval between 0 and one sampling period $t_s = T/N$ ($\tau = \mathrm{U}[0, t_s]$) and so the probability density function is:

$$f_\tau(t) = \begin{cases} \frac{1}{t_s} & 0 \le t \le t_s \\ 0 & \text{otherwise} \end{cases}$$

Since the sampling distortion error $\epsilon_{P_{T,\tau}}$ is a function of the random variable τ, it is a random variable and it is possible to calculate its first and second moment, respectively $\mu_{1,\epsilon}$ (the mean value) and $\mu_{2,\epsilon}$. Starting from expression (19):

$$\begin{aligned} \mu_\epsilon &= E\{\epsilon_{P_{T,\tau}}\} \\ &= \int_{-\infty}^{+\infty} (A_{X_k,N} \cdot 2\cos(2\pi F_s t) + B_{X_k,N} \cdot 2\sin(2\pi F_s t)) \cdot f_\tau(t) dt \\ &= 2A_{X_k,N} \cdot \int_0^{1/F_s} \cos(2\pi F_s t) \cdot F_s dt + 2B_{X_k,N} \cdot \int_0^{1/F_s} \sin(2\pi F_s t) \cdot F_s dt \\ &= 0 + 0 \\ &= 0 \end{aligned} \tag{A.5}$$

$$\begin{aligned} \mu_{2,\epsilon} &= E\{\epsilon^2_{P_{T,\tau}}\} \\ &= E\{\left(A_{X_k,N} \cdot 2\cos(2\pi F_s t) + B_{X_k,N} \cdot 2\sin(2\pi F_s t)\right)^2\} \\ &= E\{4A^2_{X_k,N} \cdot \cos^2(2\pi F_s t)\} + E\{4B^2_{X_k,N} \cdot \sin^2(2\pi F_s t)\} + E\{8A_{X_k,N} B_{X_k,N} \cos(2\pi F_s t)\sin(2\pi F_s t)\} \\ &= E\{2A^2_{X_k,N} \cdot (1 + \cos(4\pi F_s t))\} + E\{2B^2_{X_k,N} \cdot (1 - \cos(4\pi F_s t))\} + E\{4A_{X_k,N} B_{X_k,N} \sin(4\pi F_s t)\} \\ &= 2A^2_{X_k,N} + 0 + 2B^2_{X_k,N} + 0 + 0 \\ &= 2\left(A^2_{X_k,N} + B^2_{X_k,N}\right) \end{aligned} \tag{A.6}$$

The variance σ^2_ϵ is the difference between the second moment and the square of the first moment; the latter being zero, it is equal to the second moment $\mu_{2,\epsilon}$ (A.6).

A.3. Probability density function of the sampling distortion error on the pulse power estimation

The explicit expression of the power estimation error (19) as a function of the random variable τ and the probability density function of τ, $f_\tau(t)$, are known. The probability density function of $\epsilon_{P_{T,\tau}}$ can then be calculated, since it is a transformation of τ and the fundamental theorem of random variable transformation can be applied:

$$f_\epsilon(\varepsilon) = \sum_i \frac{f_\tau(t_i)}{|\epsilon'(t_i)|} \tag{A.7}$$

where t_i is the set of the solutions to the equation $\epsilon(t) = \varepsilon$:

$$A_{X_k,N} \cdot 2\cos(2\pi F_s t) + B_{X_k,N} \cdot 2\sin(2\pi F_s t) = \varepsilon \tag{A.8}$$

The Eq. (A.8) can be solved and has two solutions:

$$t_{1,2} = \frac{1}{F_s \pi} \arctan\left(\frac{4B_{X_k,N} \pm \sqrt{16A^2_{X_k,N} + 16B^2_{X_k,N} - 4\varepsilon^2}}{2\left(2A_{X_k,N} + \varepsilon\right)}\right) \tag{A.9}$$

Combining the power estimation error expression (19), the solutions described in the expression (A.9) and the probability density function of the uniformly distributed sampling delay with the probability density function transformation formula (A.7), the result is the probability density function for the power estimation error (A.10), as a function of the signal, the sampling frequency and the sampling delay. See Fig. 4 for the probability density function of the Gaussian pulse described in Section 4.1.

$$\begin{aligned} f_\epsilon(\varepsilon) &= d(p_1(\varepsilon))^{-1} + d(p_2(\varepsilon))^{-1} \\ d(p) &\doteq |4\pi\left(B_{X_k,N}\cos(2\arctan(p)) - A_{X_k,N}\sin(2\arctan(p))\right)| \\ p_{1,2} &\doteq \frac{4B_{X_k,N} \pm \sqrt{16A^2_{X_k,N} + 16B^2_{X_k,N} - 4\varepsilon^2}}{2\left(2A_{X_k,N} + \varepsilon\right)} \end{aligned} \tag{A.10}$$

Appendix B. Propagation of the Gaussian noise in the power estimation

The system noise is modeled as a zero-mean real Gaussian variable v_i with variance σ^2_v, added to the signal. The sampling delay is a random uniformly distributed variable, so the sampled sequence is not deterministic. The power estimation, affected by noise, is expressed in Eq. (24). The error term due to noise is:

$$\eta = \frac{1}{N} \sum_{n=0}^{N-1} \left(v_n^2 + 2\hat{x}_n v_n\right) \tag{B.1}$$

Before calculating the mean value and the variance of the error η, here are listed the hypotheses on the signals:

1. The noise variable v_i is zero-mean;
2. The observations of the noise variable v_i are independent and identically distributed;
3. The signal samples $\hat{x}_i$ and the noise variable v_i are independent.

And here are remembered some of the properties of the expectation, variance and covariance operators used below:

1. If X and Y are independent random variable, the expectation of their product is the product of their expectations:

$$\mathrm{E}[XY] = \mathrm{E}[X]\,\mathrm{E}[Y] \tag{B.2}$$

2. If X and Y are independent random variable, the variance of their product is:

$$\mathrm{Var}[XY] = \left(\mathrm{Var}[X] + \mathrm{E}[X]^2\right)\left(\mathrm{Var}[Y] + \mathrm{E}[Y]^2\right) - \mathrm{E}[X]^2\,\mathrm{E}[Y]^2 \tag{B.3}$$

3. The covariance of two random variables X and Y can be expressed as:

$$\mathrm{Cov}\left[X,Y\right] = \mathrm{E}\left[XY\right] - \mathrm{E}\left[X\right]\mathrm{E}\left[Y\right] \tag{B.4}$$

4. The variance of the sum of random variables X_i can be expressed as:

$$\mathrm{Var}\left[\sum_{i=1}^{N} X_i\right] = \sum_{i=1}^{N} \mathrm{Var}\left[X_i\right] + 2 \sum_{1\le i<j\le N} \mathrm{Cov}\left[X_i, X_j\right] \tag{B.5}$$

Exploiting the linearity of the expectation operator, the expectation of the error η can be manipulated as follows:

$$\begin{aligned}\mu_\eta &= \mathrm{E}\left[\frac{1}{N}\sum_{n=0}^{N-1} v_n^2 + \frac{1}{N}\sum_{n=0}^{N-1} 2\hat{x}_n v_n\right] \\ &= \frac{1}{N}\sum_{n=0}^{N-1} \mathrm{E}\left[v_n^2\right] + \frac{1}{N}\sum_{n=0}^{N-1} 2\mathrm{E}\left[\hat{x}_n v_n\right]\end{aligned} \tag{B.6}$$

Since the noise variable v_i is zero-mean, the expectation of its squared value is its variance σ_v^2. Then, being the signal and the noise independent, the expectation of their product is the product of their expectations, and the noise expectation is zero by definition. So the value of the expectation of the distortion η on the power estimation, due to noise, is:

$$\mu_\eta = \sigma_v^2 \tag{B.7}$$

The variance of the error η can be manipulated as well, applying the variance operator properties:

$$\begin{aligned}\sigma_\eta^2 &= \mathrm{Var}\left[\frac{1}{N}\sum_{n=0}^{N-1}\left(v_n^2 + 2\hat{x}_n v_n\right)\right] \\ &= \frac{1}{N^2}\sum_{n=0}^{N-1} \mathrm{Var}\left[v_n^2 + 2\hat{x}_n v_n\right] \\ &\quad + \frac{2}{N^2}\sum_{0\le n<m\le N-1} \mathrm{Cov}\left[v_n^2 + 2\hat{x}_n v_n, v_m^2 + 2\hat{x}_m v_m\right]\end{aligned} \tag{B.8}$$

Breaking the expression, each term of the sum can be further simplified.

About the argument of the first sum:

$$\mathrm{Var}\left[v_n^2 + 2\hat{x}_n v_n\right] = \mathrm{Var}\left[v_n^2\right] + \mathrm{Var}\left[2\hat{x}_n v_n\right] + \mathrm{Cov}\left[v_n^2, 2\hat{x}_n v_n\right] \tag{B.9}$$

The covariance term in (B.9) results to be 0 under the hypotheses on the noise variable (the odd moments of a Gaussian variable are 0) an on the independence between noise and signal:

$$\begin{aligned}\mathrm{Cov}\left[v_n^2, 2\hat{x}_n v_n\right] &= \mathrm{E}\left[2\hat{x}_n v_n^3\right] - \mathrm{E}\left[v_n^2\right]\mathrm{E}\left[2\hat{x}_n v_n\right] \\ &= \mathrm{E}\left[2\hat{x}_n\right]\mathrm{E}\left[v_n^3\right] - 2\sigma_v^2 \mathrm{E}\left[\hat{x}_n\right]\mathrm{E}\left[v_n\right] \\ &= 0 - 0 \\ &= 0\end{aligned} \tag{B.10}$$

Moving the analysis to the argument of the second sum in (B.8), applying the property (B.4), it results:

$$\begin{aligned}&\mathrm{Cov}\left[v_n^2 + 2\hat{x}_n v_n, v_m^2 + 2\hat{x}_m v_m\right] = \\ &= \mathrm{E}\left[v_n^2 v_m^2 + 2\hat{x}_n v_n v_m^2 + 2\hat{x}_m v_m v_n^2 + 4\hat{x}_n v_n \hat{x}_m v_m\right] \\ &\quad - \mathrm{E}\left[v_n^2 + 2\hat{x}_n v_n\right]\mathrm{E}\left[v_m^2 + 2\hat{x}_m v_m\right]\end{aligned} \tag{B.11}$$

Applying then property (B.2) and the linearity of the expectation operator, remembering that v_i is an i.i.d. variable and that it is independent with respect to the signal $\hat{x}_i$, it follows that:

$$\begin{aligned}&\mathrm{Cov}\left[v_n^2 + 2\hat{x}_n v_n, v_m^2 + 2\hat{x}_m v_m\right] = \\ &= \mathrm{E}\left[v_n^2\right]\mathrm{E}\left[v_m^2\right] + \mathrm{E}\left[2\hat{x}_n\right]\mathrm{E}\left[v_n\right]\mathrm{E}\left[v_m^2\right] \\ &\quad + \mathrm{E}\left[2\hat{x}_m\right]\mathrm{E}\left[v_m\right]\mathrm{E}\left[v_n^2\right] + \mathrm{E}\left[4\hat{x}_n\hat{x}_m\right]\mathrm{E}\left[v_n\right]\mathrm{E}\left[v_m\right] \\ &\quad - \left(\mathrm{E}\left[v_n^2\right] + \mathrm{E}\left[2\hat{x}_n\right]\mathrm{E}\left[v_n\right]\right)\left(\mathrm{E}\left[v_m^2\right] + \mathrm{E}\left[2\hat{x}_m\right]\mathrm{E}\left[v_m\right]\right)\end{aligned} \tag{B.12}$$

Since the noise v_i is zero-mean, the covariance is finally zero:

$$\begin{aligned}&\mathrm{Cov}\left[v_n^2 + 2\hat{x}_n v_n, v_m^2 + 2\hat{x}_m v_m\right] = \\ &= \mathrm{E}\left[v_n^2\right]\mathrm{E}\left[v_m^2\right] + 0 + 0 + 0 - \left(\mathrm{E}\left[v_n^2\right] + 0\right)\left(\mathrm{E}\left[v_m^2\right] + 0\right) \\ &= 0\end{aligned} \tag{B.13}$$

So, using the results (B.9), (B.10), and (B.13) to simplify the expression (B.8), the variance of the error η can be written as:

$$\sigma_\eta^2 = \frac{1}{N^2}\sum_{n=0}^{N-1} \mathrm{Var}\left[v_n^2\right] + \frac{1}{N^2}\sum_{n=0}^{N-1} \mathrm{Var}\left[2\hat{x}_n v_n\right] \tag{B.14}$$

The argument of the first sum in (B.14), the variance of the square of the zero-mean Gaussian variable v_n, is a function of the variance σ_v^2:

$$\begin{aligned}\mathrm{Var}\left[v_n^2\right] &= \mathrm{E}\left[\left(v_n^2 - \sigma_v^2\right)^2\right] \\ &= \mathrm{E}\left[v_n^4 + \sigma_v^4 - 2v_n^2\sigma_v^2\right] \\ &= \mathrm{E}\left[v_n^4\right] + \sigma_v^4 - 2\mathrm{E}\left[v_n^2\right]\sigma_v^2 \\ &= 3\sigma_v^4 + \sigma_v^4 - 2\sigma_v^2\sigma_v^2 \\ &= 2\sigma_v^4\end{aligned} \tag{B.15}$$

The argument of the second sum in (B.14), the variance of the product between the signal sample and the added noise, can be rewritten as:

$$\begin{aligned}\mathrm{Var}\left[2\hat{x}_n v_n\right] &= \left(\mathrm{Var}\left[2\hat{x}_n\right] + \mathrm{E}\left[2\hat{x}_n\right]^2\right)\left(\mathrm{Var}\left[v_n\right] + \mathrm{E}\left[v_n\right]^2\right) \\ &\quad - \mathrm{E}\left[2\hat{x}_n\right]^2 \mathrm{E}\left[v_n\right]^2 \\ &= \left(\mathrm{Var}\left[2\hat{x}_n\right] + \mathrm{E}\left[2\hat{x}_n\right]^2\right)\left(\sigma_v^2 + 0\right) - \mathrm{E}\left[2\hat{x}_n\right]^2 \cdot 0 \\ &= 4\left(\mathrm{Var}\left[\hat{x}_n\right] + \mathrm{E}\left[\hat{x}_n\right]^2\right)\sigma_v^2\end{aligned} \tag{B.16}$$

The signal sample $\hat{x}_n$ is the signal sample $x(nt_s + \tau)$ with sampling delay τ, random uniformly distributed variable in the range $[0, t_s]$. The expectation and variance of $\hat{x}_n$ are unknown. A possible assumption is that $x(nt_s+\tau)$ might be linearized on the sampling interval and the mean value would be $x((n+1/2)t_s)$. A second assumption is that the variance of the single sample caused by the sampling phase variation is much smaller than the sample mean value. Both approximations' accuracy increases with the sampling frequency, where the noise contribution gets significant with respect to the sampling distortion contribution to the power estimation error. Under these assumptions, the error η variance can finally be expressed and approximated as:

$$\begin{aligned}\sigma_\eta^2 &= \frac{2}{N}\sigma_v^4 + \frac{4}{N^2}\sigma_v^2 \sum_{n=0}^{N-1}\left(\mathrm{Var}\left[\hat{x}_n\right] + \mathrm{E}\left[\hat{x}_n\right]^2\right) \\ &\simeq \frac{2}{N}\sigma_v^4 + \frac{4}{N^2}\sigma_v^2 \sum_{n=0}^{N-1} x\left((n+1/2)t_s\right)^2 \\ &\simeq \frac{2}{N}\sigma_v^4 + \frac{4}{N}\sigma_v^2 P_T\end{aligned} \tag{B.17}$$

The sum of the square of the N samples of the noiseless signal is the estimator of the pulse power P_T in the noiseless case. Approximating such a sum with P_T itself is the more accurate the higher is the sampling frequency. What is neglected with this approximation is in the order of the product of the noise power with the single sample variance.

References

[1] R.E. Shafer, Beam position monitoring, AIP Conf. Proc. 212 (1990) 26.

[2] C.E. Shannon, A mathematical theory of communication, Bell Syst. Tech. J. 27 (3) (1948) 379–423.

[3] C.E. Shannon, Communication in the presence of noise, in: Proceedings of the IRE, Vol. 37, IEEE, 1949, pp. 10–21.

[4] M.B. Matthews, On the linear minimum-mean-squared-error estimation of an undersampled wide-sense stationary random process, IEEE Trans. Signal Process. 48 (1) (2000) 272–275.

[5] A. Kipnis, A.J. Goldsmith, Y.C. Eldar, T. Weissman, Distortion rate function of sub-Nyquist sampled Gaussian sources, IEEE Trans. Inf. Theory 62 (1) (2016) 401–429.

[6] E. Mohammadi, F. Marvasti, Sampling and distortion tradeoffs for bandlimited periodic signals, IEEE Trans. Inf. Theory 64 (3) (2018) 1706–1724.

[7] A. Kipnis, Y.C. Eldar, A.J. Goldsmith, Fundamental distortion limits of analog-to-digital compression, IEEE Trans. Inf. Theory 64 (9) (2018) 6013–6033.
[8] R.H. Walden, Analog-to-digital converter survey and analysis, IEEE J. Sel. Areas Commun. 17 (4) (1999) 539–550.
[9] Texas instrument ADS54J60 data-sheet, 2019, [cited 2020-04-06]. URL http://www.ti.com/lit/ds/symlink/ads54j60.pdf.
[10] Analog devices, Inc. AD9680 data-sheet, 2019, [cited 2020-04-06]. URL https://www.analog.com/media/en/technical-documentation/data-sheets/AD9680.pdf.
[11] Analog devices, Inc. AD9689 data-sheet, 2017, [cited 2020-04-06]. URL https://www.analog.com/media/en/technical-documentation/data-sheets/AD9689.pdf.
[12] Texas instrument ADC12DJ3200 data-sheet, 2017, [cited 2020-04-06]. URL http://www.ti.com/lit/ds/symlink/adc12dj3200.pdf.
[13] Teledyne e2v semiconductors SAS EV12AQ600 data-sheet, 2020, [cited 06.04.2020]. URL https://www.teledyne-e2v.com/shared/content/resources/File/documents/broadband-data-converters/EV12AQ600/DS%2060S%20218366%20EV12AQ60x%20revB.pdf.